Environmental Science & Technology

pubs.acs.org/est

Article

Stimulated Raman Scattering Microscopy Reveals Bioaccumulation of Small Microplastics in Protozoa from Natural Waters

Mei Wang,[#] Zhiliang Huang,[#] Chao Wu, Shuai Yan, Hai-Tao Fang, Wei Pan, Qiao-Guo Tan, Ke Pan, Rong Ji, Liuyan Yang, Bingcai Pan, Ping Wang,* and Ai-Jun Miao*

Cite This: *Environ. Sci. Technol.* 2024, 58, 2922−2930

Read Online

ACCESS | Metrics & More | Article Recommendations | Supporting Information

ABSTRACT: Microplastics (MPs) are pollutants of global concern, and bioaccumulation determines their biological effects. Although microorganisms form a large fraction of our ecosystem's biomass and are important in biogeochemical cycling, their accumulation of MPs has never been confirmed in natural waters because current tools for field biological samples can detect only MPs > 10 μm. Here, we show that stimulated Raman scattering microscopy (SRS) can image and quantify the bioaccumulation of small MPs (<10 μm) in protozoa. Our label-free method, which differentiates MPs by their SRS spectra, detects individual and mixtures of different MPs (e.g., polyethylene, polypropylene, polyvinyl chloride, polyethylene terephthalate, polystyrene, and poly(methyl methacrylate)) in protozoa. The ability of SRS to quantify cellular MP accumulation is similar to that of flow cytometry, a fluorescence-based method commonly used to determine cellular MP accumulation. Moreover, we discovered that protozoa in water samples from Yangtze River, Xianlin Wastewater Treatment Plant, Lake Taihu and the Pearl River Estuary accumulated MPs < 10 μm, but the proportion of MP-containing cells was low (~2−5%). Our findings suggest that small MPs could potentially enter the food chain and transfer to organisms at higher trophic levels, posing environmental and health risks that deserve closer scrutiny.

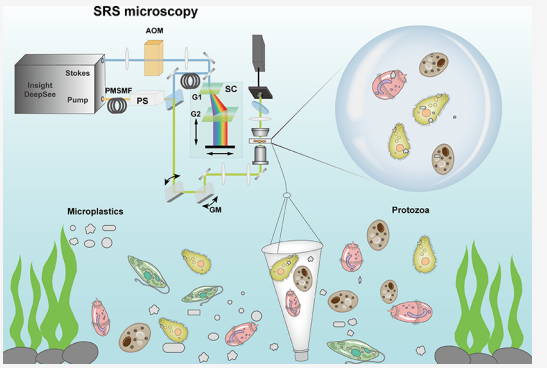

KEYWORDS: *bioaccumulation, microplastics, natural waters, protozoa, stimulated Raman scattering*

INTRODUCTION

Microplastics (MPs) are plastic particles <5 mm in size.[1] Found in nearly every environmental compartment, these pollutants are of global concern because they can accumulate in organisms and enter the food chain.[2,3] As the base of our food chain, microorganisms (such as bacteria, algae, and protozoa) form a large part of the biomass in various ecosystems and are critical in biogeochemical cycling of various elements (e.g., carbon, nitrogen, phosphorus) and pollutants.[4] While MPs have been shown to accumulate and cause adverse effects in microorganisms in the laboratory,[5,6] their accumulation in real environments has never been confirmed. Limited by the spatial resolution of available tools such as spontaneous Raman and infrared spectroscopy,[7] current field studies have largely focused only on the accumulation of MPs > 10 μm in large organisms such as fish, mussels, shrimp, and crabs.[8−10] Because small MPs (<10 μm) can traverse biological barriers more readily and may be more harmful than large MPs (>10 μm),[11] investigating the accumulation of large MPs in large organisms without knowing the behavior of small MPs in microorganisms in the natural environment may underestimate the potential risks of MPs.

The commonly detected polymers of MPs are polyethylene (PE), polypropylene (PP), polyvinyl chloride (PVC), polyethylene terephthalate (PET), polystyrene (PS), and poly(methyl methacrylate) (PMMA). It is estimated that surface waters contain thousands to millions of these MP particles per cubic meter.[12−15] Yet, most laboratory studies to date have examined only the bioaccumulation of PS. This is because tracing MPs requires labeling the polymer with either fluorescent dyes,[16,17] heavy metals,[18,19] or isotopes[20,21] and these techniques are mostly established for PS. The problem is that labels can dissociate[22] and labeling techniques cannot be developed fast enough for the ever growing numbers of MPs.[23] Because MPs in the natural environment are unlabeled, using label-free methods could simplify the investigation process and broaden the types of MPs that are detected.

Stimulated Raman scattering microscopy (SRS) is an attractive label-free optical imaging technique for identifying MPs. It coherently excites selected molecular vibrations through a nonlinear process resembling stimulated emissions.[24,25] Because its stimulation factor can be as high as 1×10^6, SRS is

Received: September 11, 2023
Revised: January 9, 2024
Accepted: January 11, 2024
Published: January 31, 2024

https://doi.org/10.1021/acs.est.3c07486
Environ. Sci. Technol. 2024, 58, 2922−2930

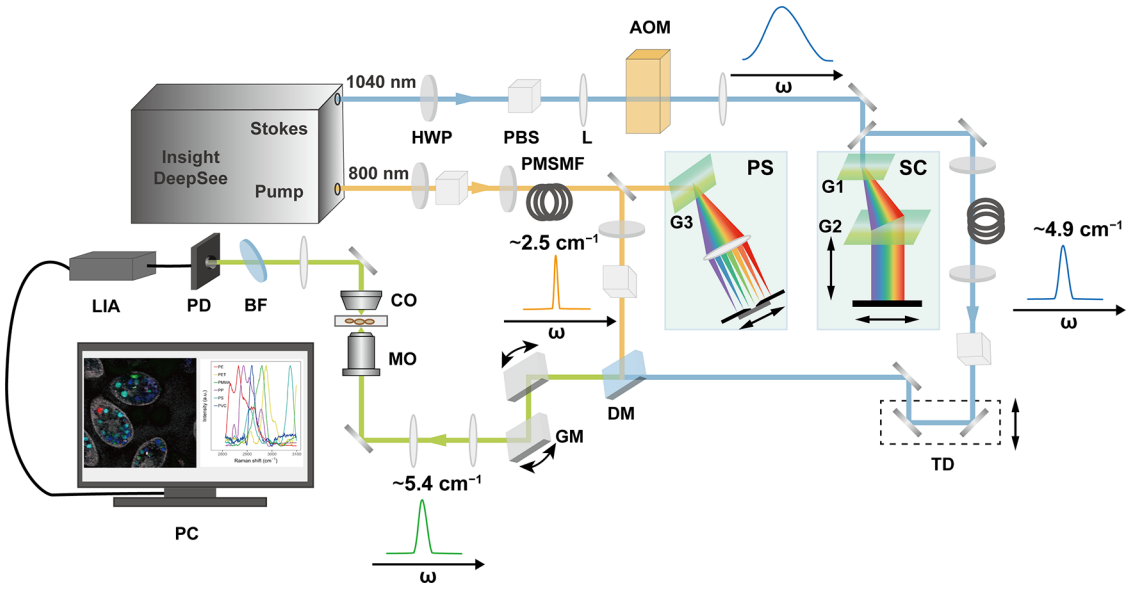

Figure 1. Schematic of SRS microscopy. PS: pulse shaper consisting of holographic grating, achromatic lens, and slit whose ultimate spectral resolution can reach 2.5 cm^{-1}. SC: spectral compressor consisting of a grating pair with a distance of 15 cm and a 15 m long PMSMF whose ultimate spectral resolution can reach 4.87 cm^{-1} when the Stokes laser power is 425 mW. HWP: half-wave plate, PBS: polarizing beam splitter, L: lens; AOM: acousto-optical modulator, G: grating, TD: time delay, PMSMF: polarization-maintaining single-mode fiber, DM: dichroic mirror, GM: galvo mirror, MO: microscope objective; CO: condenser, BF: band-pass filter; PD: photodiode, LIA: lock-in amplifier; PC: personal computer.

orders of magnitude faster and more sensitive than conventional Raman microscopy. The method has been used to examine the bioaccumulation of nanoparticles in cells[26] and protozoa.[27] Zada et al.[28] have also previously used SRS to identify various MPs (including nylon, PET, PS, PP, and PE) in the sediments of the Rhine estuary. While promising, for SRS to be a relevant method for monitoring the vast number and variety of MPs in the environment, its spectral information must expand beyond the five calibrated polymers reported previously[28] and its resolution must go below 12 μm as the detection limit in Zada et al.[28] for it to identify smaller MPs that are likely to be taken up by highly endocytic microorganisms such as protozoa. In the aquatic environment, protozoans are important grazers of microbes with critical roles in food chains, nutrient turnovers, and as bioindicators of pollution and biocontrol agents.[29,30]

Here, using an improved homemade system reported previously (Figure 1),[31] we show that SRS can be used to visualize and quantify the bioaccumulation of individual or a mixture of PS, PVC, PP, PE, PET, and PMMA MPs (<10 μm) in protozoa. Our system differentiates the polymers based on their SRS spectra between 2800 and 3100 cm^{-1} rather than on the specific wavenumber of each type of MPs.[28,32] With a spectral resolution of 5.4 cm^{-1} and spatial resolution of 400 nm in theory, we detected MPs in laboratory grown *Tetrahymena thermophila* and discovered PE and unidentified MPs < 10 μm in various protozoa found in water samples collected from Yangtze River (third longest river in the world), the Xianlin Wastewater Treatment Plant, Lake Taihu (third largest freshwater lake in China), and the Pearl River Estuary (one of China's largest estuaries with strong anthropogenic impacts). Our results show that small MPs are widely distributed in different natural waters, necessitating a closer examination of their impacts.

MATERIALS AND METHODS

Microplastics. The six types of MPs used in this study were PE (Bowen Plastic Chemical Co. Ltd., Shanghai, China), PET (Hongcheng New Material Co. Ltd., Guangdong, China), PMMA (Rigor Technology Co. Ltd., Jiangsu, China), PP (Wanda Plastic Material, Guangdong, China), and PVC (Wanda Plastic Material, Guangdong, China). PS with sizes of approximately 50 (55 ± 6 nm), 100 (113 ± 9 nm), 200 (200 ± 8 nm), 500 (425 ± 30 nm), and 3000 nm (2728 ± 103 nm) were synthesized by adding different amounts of the emulsifier sodium dodecyl sulfate and the initiator ammonium persulfate during the polymerization.[33] The morphology of the MPs was visualized by scanning electron microscopy (Quanta FEG 250, FEI, USA). Their chemical composition was determined by Fourier transform infrared (FT-IR) (Tensor 27, Bruker, Germany) and Raman spectroscopy (XploRA PLUS, Horiba, France).

Cell Culture. *Tetrahymena thermophila* SB210 was obtained from the Institute of Hydrobiology (Chinese Academy of Sciences, Wuhan, China) and maintained in SPP medium at 24 ± 1 °C.[34] Potential effects of undefined components in SPP medium on the dispersibility of the MPs were excluded by performing the exposure experiments (described below) in Dryl's medium (2 mM NaH_2PO_4, 1 mM Na_2HPO_4, and 1.5 mM $CaCl_2$ at pH 6.9).[27] Before each exposure experiment, *T. thermophila* cells were cultured in SPP medium until they reached the midexponential growth phase, at which time they were collected by centrifugation (1700 × *g*, 10 min), rinsed with freshly prepared Dryl's medium, and resuspended in exposure medium.

Microplastic Exposure Experiments. Five exposure experiments were performed: (1) *T. thermophila* cells (1×10^5 cells/mL) were exposed to 100 mg PE-, PET-, PMMA-, PP-, PS-, or PVC-MPs/L for 120 min; (2) *T. thermophila* cells were exposed simultaneously to 100 mg each of PE-, PET-, PMMA-, PP-, and PVC-MPs/L and 20 mg PS-MPs/L for 120 min; (3) *T. thermophila* cells were exposed to 0.16, 0.8, 4, 20, or 100 mg PS-MPs/L for 120 min; (4) *T. thermophila* cells were exposed to 20 mg 50-, 100-, 200-, 500-, 1000-, or 3000 nm PS-MPs/L for 120 min; (5) *T. thermophila* cells were exposed to 20 mg PS-MPs/L for 15, 30, 60, and 90 min. The size of the PS-MPs used in the

https://doi.org/10.1021/acs.est.3c07486
Environ. Sci. Technol. 2024, 58, 2922−2930

experiments described above was 500 nm unless specified otherwise. At each time point of the exposure experiments, 2 mL of cell suspension was collected, fixed in paraformaldehyde (final concentration 2% w/v), and stored at 4 °C until imaged by SRS as described below. In experiment (5), *T. thermophila* cells were also exposed to fluorescently labeled 500 nm PS-MPs at a concentration of 20 mg/L for 15, 30, 60, and 90 min. At each time point, 0.5 mL of cell suspension was collected and the cellular accumulation of PS-MPs was determined by flow cytometry (BD, NJ, USA), as reported in our previous study.[35]

Field Sample Collection. Protozoa were collected from the Yangtze River near Bagua Zhou (32.24203 N, 118.82989 E), the aeration tank of the Xianlin Wastewater Treatment Plant (32.15018 N, 118.94810 E), the Meiliang Bay of Lake Taihu (31.50650 N, 120.13444 E), and the coastal water of the Pear River Estuary (22.54687 N, 113.89402 E) as shown in the map of Figure S1. Yangtze River was chosen because it is the third longest river in the world and the sampling site in Yangtze River is close to a chemical industry park. The wastewater treatment plant we chose herein mainly treats urban domestic sewage. Lake Taihu was chosen because it is the third largest freshwater lake in China and the sampling site is in Meiliang Bay, which is the one of the most polluted area in Lake Taihu.[36] The coastal water was collected from the Pearl River Estuary, which is one of China's largest estuaries with strong anthropogenic impacts.[37] For this purpose, a cone-shaped plankton net (mesh size of 65 μm) with a collecting vessel at the narrow end was used to collect protozoa from the surface water (0.1−0.5 m below the surface) following a procedure similar to that recommended by the US EPA.[38] The samples collected from each site were divided in half, with one-half fixed in paraformaldehyde (final concentration 2% w/v) on site and stored at 4 °C until SRS imaging and the other half left unfixed but sent to the laboratory immediately to be examined by conventional compound microscopy.

SRS Imaging. The SRS microscope contained a dual-output femtosecond laser (InSight DeepSee, Spectra-Physics, Newport, USA) with a repetition rate of 80 MHz. The pulse width of the 800 nm pump laser was 120 fs, and the laser was coupled to a 0.3 m polarization-maintaining single-mode fiber (PMSMF). After the pump laser had transmitted the beam to a 4f pulse shaper system, consisting of a grating (1800 l/mm@840 nm, Wasatch Photonics, UT, USA), a lens, and a slit with a mirror on a motorized stage, pulses were delivered with a pulse width of ~2.5 ps, as measured by an autocorrelator (CARPE, APE). The pulse width of the 1040 nm Stokes laser was 220 fs, with the laser pulses sent to a spectral compressor after modulation of the laser beam by an acousto-optic modulator at a frequency of 2.7 MHz. The spectral compressor consisted of a grating pair (1000 l/mm, LSFSG-1000, LightSmyth, OR, USA) with a distance of 15 cm and a 15 m PMSMF for self-phase modulation. The pulse width of the Stokes laser (~6.5 ps) was measured through the two-photon signal of rhodamine 6G, using a time-delay module. A dichroic mirror (DMSP1000L, Thorlabs, NJ, USA) and a time-delay module were used to combine the pump and probe beams spatially and temporally. The lasers were delivered to a 2D galvanometer for SRS imaging; two short-pass filters (ET980sp, Chroma, VT, USA) were used to block the stokes beam. The objective lens we used (UPLSAPO 60XW) has a magnification of 60× and its numerical aperture (NA) is 1.2. After interaction with the sample, the transmission laser was collected by using a high NA (1.4) oil condenser (U-AAC, Olympus). A homemade photodiode with resonant and lock-in amplifiers (HF2 LI, Zurich Instruments, Switzerland) was used to detect the SRS signal.[31] The Labview platform synchronized wavelength scanning with stacking of the X-Y-Ω images. The powers for pump and Stokes lasers were 3 and 300 mW, respectively, before the galvanometer and were 1.5 and 150 mW, respectively, at the sample. The mapping step size was 800 nm, and the dwell time was 10 μs unless otherwise specified. Hyperspectral SRS imaging was performed by varying the Raman shift from 2800 to 3100 cm^{-1}, thus covering the C−H stretching bands of proteins and lipids as well as the stretching bands of the different MPs. The fingerprint spectra in the range of 800 to 1800 cm^{-1} can also distinguish the different MPs. But their intensity is relatively weak, and thus the detection limit is not as good as those in the range of 2800 and 3100 cm^{-1}. While the detection limit can be improved by increasing the laser power, this may burn and destroy the biological sample. Even though the wavenumber we used herein was between 2800 and 3100 cm^{-1}, there is still a need to increase the pulse width to reduce the transient power of the laser so that we can image protozoan cells without burning the sample.

After SRS data acquisition, the multivariate curve resolution (MCR) algorithm was used to decompose the three-dimensional SRS imaging data matrix **D** (X-Y-Ω) into signal intensity profiles and the Raman spectra of the principal components, represented by matrices **C** and $\mathbf{S}^{\mathbf{T}}$ in eq 1, where **T** is the transpose of the matrix **S** and **E** is the residual matrix or experimental error.

$$\mathbf{D} = \mathbf{C}\cdot\mathbf{S}^{\mathbf{T}} + \mathbf{E} \quad (1)$$

The MCR input is the 3D matrix **D** and the reference spectrum of each component. **S** contains the output spectra of all fitted components related to the reference spectrum. Based on an initial estimate of the pure spectra from a principal component analysis or prior knowledge, an alternating least-squares algorithm calculates **C** and **S** according to eq 1 iteratively until the results optimally fit the data matrix **D**. Since the inputs to MCR require both data set and the initial estimation of SRS spectra for major components, a *k*-means clustering algorithm is employed to partition all SRS spectra of each pixel into groups, and the spectra of each group are then used as initial spectral estimation for the MCR algorithm.

RESULTS AND DISCUSSION

SRS Detects Individual and Mixture of MPs. We first tested the ability of SRS to image a mixed suspension of 100 mg of PE-, PET-, PMMA-, PP-, PS-, and PVC-MPs/L (based on carbon weight). MPs obtained by polymerization (PMMA and PS) and phase separation (PVC and PP) are spherical, while those obtained by ball-milling (PE and PET) have irregular shapes. All six MPs dispersed well in Dryl's experimental medium and their primary particle size ranged from 211 to 16698 nm (see the Supporting Information and Figure S2 for detailed physicochemical characterization of the MPs).

SRS spectral differences of the polymers between 2800 and 3100 cm^{-1} (Figure S2d) obtained through the integration of hyperspectral SRS imaging, *k*-means clustering, and MCR analysis enabled label-free imaging of PE-, PET-, PMMA-, PP-, PS-, and PVC-MPs.[39] As mentioned before, MCR is a bilinear model that decomposes the SRS spectral data set and outputs SRS signal intensity maps and Raman spectra of the principal components. The signal intensity of a component at each pixel in the map is expressed as a percentage relative to the intensity of the MCR-optimized spectrum. A hyperspectral stack of 250 images at wavenumbers between 2800 and 3100 cm^{-1} was

https://doi.org/10.1021/acs.est.3c07486
Environ. Sci. Technol. 2024, 58, 2922−2930

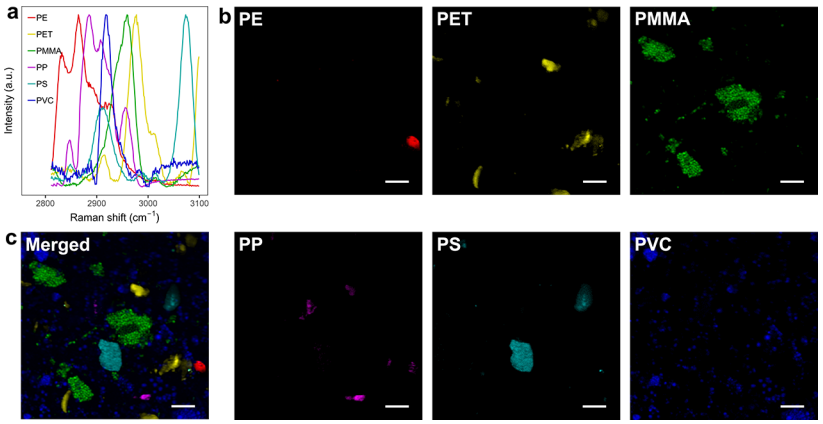

Figure 2. SRS imaging of a mixture of microplastics (MPs) in experimental medium. (a) SRS spectra of a mixture of 100 mg PE-, PET-, PMMA-, PP-, PS-, and PVC-MPs/L in Dryl's medium (2 mM NaH_2PO_4, 1 mM Na_2HPO_4, and 1.5 mM $CaCl_2$ with pH 6.9). (b, c) Individual (b) and merged (c) SRS signal intensity maps of PE-, PET-, PMMA-, PP-, PS-, and PVC-MPs in the same field of view. In the maps, the signal intensity of each type of MP at each pixel is expressed as the percentage relative to the intensity of the multivariate curve resolution (MCR)-optimized spectrum. Scale bars, 10 μm.

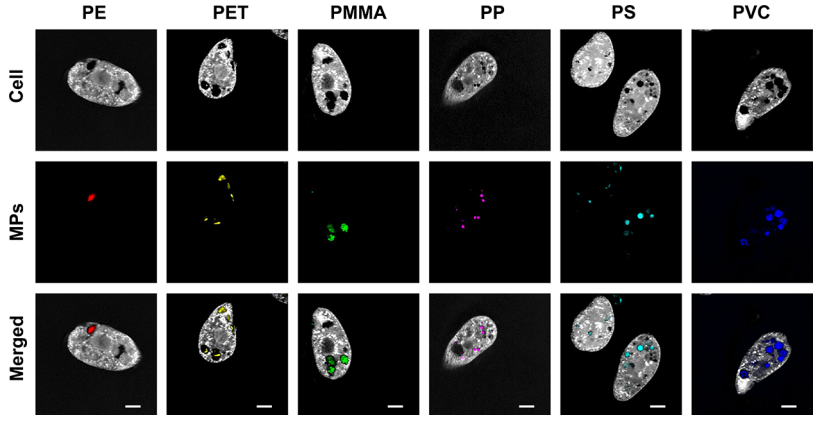

Figure 3. SRS imaging of *T. thermophila* exposed to a single type of MP. The top row shows the outline of *T. thermophila* cells exposed to 100 mg PE-, PET-, PMMA-, PP-, PS-, or PVC-MPs/L in Dryl's medium (2 mM NaH_2PO_4, 1 mM Na_2HPO_4, and 1.5 mM $CaCl_2$ with pH 6.9) for 120 min, as indicated by the SRS signal intensity maps of proteins and lipids. The middle row is the SRS signal intensity maps of the different types of MPs as accumulated in the *T. thermophila* cells of the top row, and the bottom row is the merged SRS signal intensity maps of the proteins, lipids, and the corresponding MPs in the same field of view as that shown in the top and middle rows. In the maps, the signal intensity of each component (i.e., proteins, lipids, or MP) at each pixel is expressed as the percentage relative to the intensity of the MCR-optimized spectrum. Scale bars, 10 μm.

acquired in 400 s (Supplementary Movie 1). Analyzing the X-Y-Ω (Ω: Raman shift) image stack using the MCR algorithm, we retrieved both the spectra (Figure 2a) and SRS signal intensity maps for PE, PET, PMMA, PP, PS, and PVC (Figure 2b). The MCR-optimized spectra for all 6 MPs matched their individual SRS spectra in Figure S2d. Overlay of all SRS signal intensity maps is shown in Figure 2c. These results demonstrate that SRS can image mixed suspension of MPs.

SRS Imaging of MPs in Laboratory Grown Protozoa. To investigate whether SRS can be used to visualize the bioaccumulation of MPs in protozoa, we exposed laboratory grown *T. thermophila* to 100 mg/L of either PE, PET, PMMA, PP, PS, or PVC MPs for 120 min before collecting and analyzing the hyperspectral SRS images of the exposed organisms using the MCR algorithm. The outline of *T. thermophila* is constructed from the SRS signal intensity map of its proteins and lipids that generated C−H vibration Raman peaks at 2490 and 2935 cm^{-1} (Figure 3, top row).[27] All 6 MPs accumulated significantly in the food vacuoles of *T. thermophila* (Figure 3, middle and bottom row).

Because natural environments contain a variety of MPs,[40] more than one type of MP is likely to accumulate in the organisms. To examine whether SRS can identify different types of MPs that accumulate in the protozoa, we exposed *T. thermophila* to a mixture containing 100 mg/L each of PE-, PET-, PMMA-, PP-, and PVC-MPs and 20 mg/L of PS. A lower concentration of PS was applied because our preliminary experiment shows that PS accumulates more readily in *T. thermophila* than other MPs. This difference in bioaccumulation is likely due to differences in size, shape, density, and chemical composition of the MPs.[41]

The SRS-derived signal intensity maps show all 6 MPs accumulated in *T. thermophila* (Figure 4). Although each cell can accumulate multiple types of MPs simultaneously, no single cell can accumulate all six MPs at the same time. Despite the lower concentration, PS showed the highest uptake, followed by PVC and PMMA. The low uptake seen with PP, PE, and PET MPs is likely due to their irregular shapes and broader size distribution. While further studies are needed to understand this differential accumulation of MPs, these results show SRS can simultaneously identify all 6 types of MPs in *T. thermophila* and is thus a valuable tool for studying bioaccumulation of MPs in the natural environment.

https://doi.org/10.1021/acs.est.3c07486
Environ. Sci. Technol. 2024, 58, 2922−2930

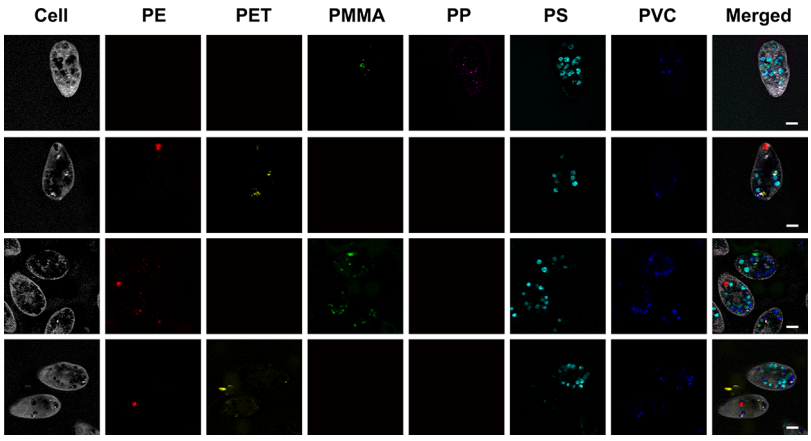

Figure 4. SRS imaging of*T. thermophila* exposed to all six types of MPs simultaneously. The first column is the outline of the representative *T. thermophila* cells simultaneously exposed to 100 mg PE-, PET-, PMMA-, PP-, and PVC-MPs/L and 20 mg PS-MPs/L in Dryl's medium (2 mM NaH_2PO_4, 1 mM Na_2HPO_4, and 1.5 mM $CaCl_2$ with pH 6.9) for 120 min, as indicated by the SRS signal intensity maps of proteins and lipids. The second to seventh columns are the SRS signal intensity maps of the different types of MPs as accumulated in the *T. thermophila* cells of the first column; the eighth column shows the merged SRS signal intensity maps of the proteins, lipids, and the corresponding MPs in the same field of view as that shown in the first to seventh columns. While each cell can simultaneously accumulate multiple types of MPs, none of the cells accumulated all 6 MPs at once. Despite the lower concentration, PS showed the highest uptake, followed by PVC and PMMA. The low uptake seen with PP, PE and PET MPs is likely due to their irregular shapes and broader size distribution. In the maps, the signal intensity of each component (proteins, lipids, or MPs) at each pixel is expressed as the percentage relative to the intensity of the MCR-optimized spectrum. Scale bars, 10 μm.

According to Li et al.,[12] the abundance of MPs in freshwater systems varies with the location, from above 1 million pieces per cubic meter to less than 1 piece in 100 m^3. Then we can estimate that the mass concentration of MPs in freshwater systems varies from 125 pg/L to 12.5 mg/L based on an average weight of 12.5 μg for an environmentally relevant MP particle.[42] A recent mathematical model[43] further predicts that by 2030, the concentration of MPs in the subtropical convergence zone will increase 2-fold. We used our SRS-based method to visualize the bioaccumulation of MPs at environmentally realistic concentrations. *T. thermophila* cells were exposed to 0.16, 0.8, 4, 20, and 100 mg PS-MPs/L (primary particle size ~500 nm) for 120 min and imaged thereafter. Significant amounts of PS-MPs accumulated in the cells at all of the tested concentrations (Figure 5a). However, as the ambient PS-MP concentration decreased from 100 to 0.16 mg/L, the dwell time of SRS imaging increased from 10 to 200 μs. At 0.16 mg/L, the intracellular concentration of PS comes close to the detection limit of our SRS because a high dwell time (or laser power) increases signal noise.[44] Given that bioaccumulation in natural environments increases over time, the exposure concentration of PS could be lowered further for exposures longer than 120 min.

Because MPs in the natural environment come in all sizes, we also exposed *T. thermophila* to 50, 100, 200, 500, and 3000 nm PS-MPs for 120 min (Figure S3). Although the size detection limit of our SRS is ~400 nm as restricted by Abbe's diffraction limit,[45] all sizes accumulated significantly in the cells (Figure 5b). Small particles (50, 100, and 200 nm) below the diffraction limit were observed as a result of their stronger SRS signal compared to the background. Additionally, they may aggregate or concentrate in micron-sized cellular compartments such as food vacuoles (~5 μm),[46] which makes them easier to be detected.

We further used SRS to monitor and quantify the bioaccumulation of PS-MPs over time. *T. thermophila* cells were exposed to 20 mg/L of 500 nm PS-MPs for 15, 30, 60, and 90 min, and SRS spectra were obtained for each time point. Accumulation of fluorescently labeled PS of the same size was

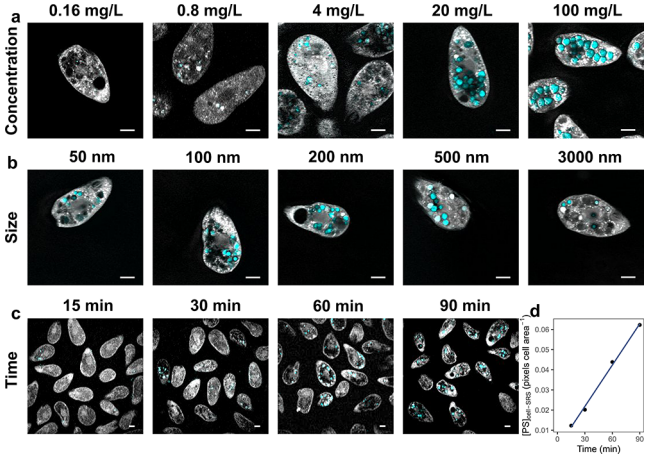

Figure 5. SRS imaging of*T. thermophila* exposed to PS-MPs. (a) SRS imaging shows that the accumulation of PS-MPs (500 nm) by *T. thermophila* cells increased as the concentration (0.16−100 mg/L) of the MPs in the exposure medium (Dryl's, 2 mM NaH_2PO_4, 1 mM Na_2HPO_4, and 1.5 mM $CaCl_2$ with pH 6.9) increased. (b) SRS imaging shows the accumulation of 50-, 100-, 200-, 500-, and 3000 nm PS-MPs in *T. thermophila* cells. (c) SRS imaging shows that the accumulation of PS-MPs (500 nm) in *T. thermophila* increased as the exposure time increased. (d) According to the results in (c), the intracellular concentration of PS-MPs ($[PS]_{cell\text{-}SRS}$), expressed as the ratio of the area of pixels identified as PS-MPs to the area of pixels identified as *T. thermophila*, increased linearly with the exposure time. In the SRS signal intensity maps of (a−c), the signal intensity of each component (i.e., proteins, lipids, or MP) at each pixel is expressed as the percentage relative to the intensity of the MCR-optimized spectrum. Scale bars, 10 μm.

examined in parallel by flow cytometry. We observed PS accumulation increasing with exposure time (Figure 5c). When the cellular concentration of PS-MPs is expressed as the ratio of the area of pixels identified as PS-MPs to the area of pixels identified as *T. thermophila*, we found a linear correlation between the cellular concentration of MPs and exposure time

https://doi.org/10.1021/acs.est.3c07486
Environ. Sci. Technol. 2024, 58, 2922−2930

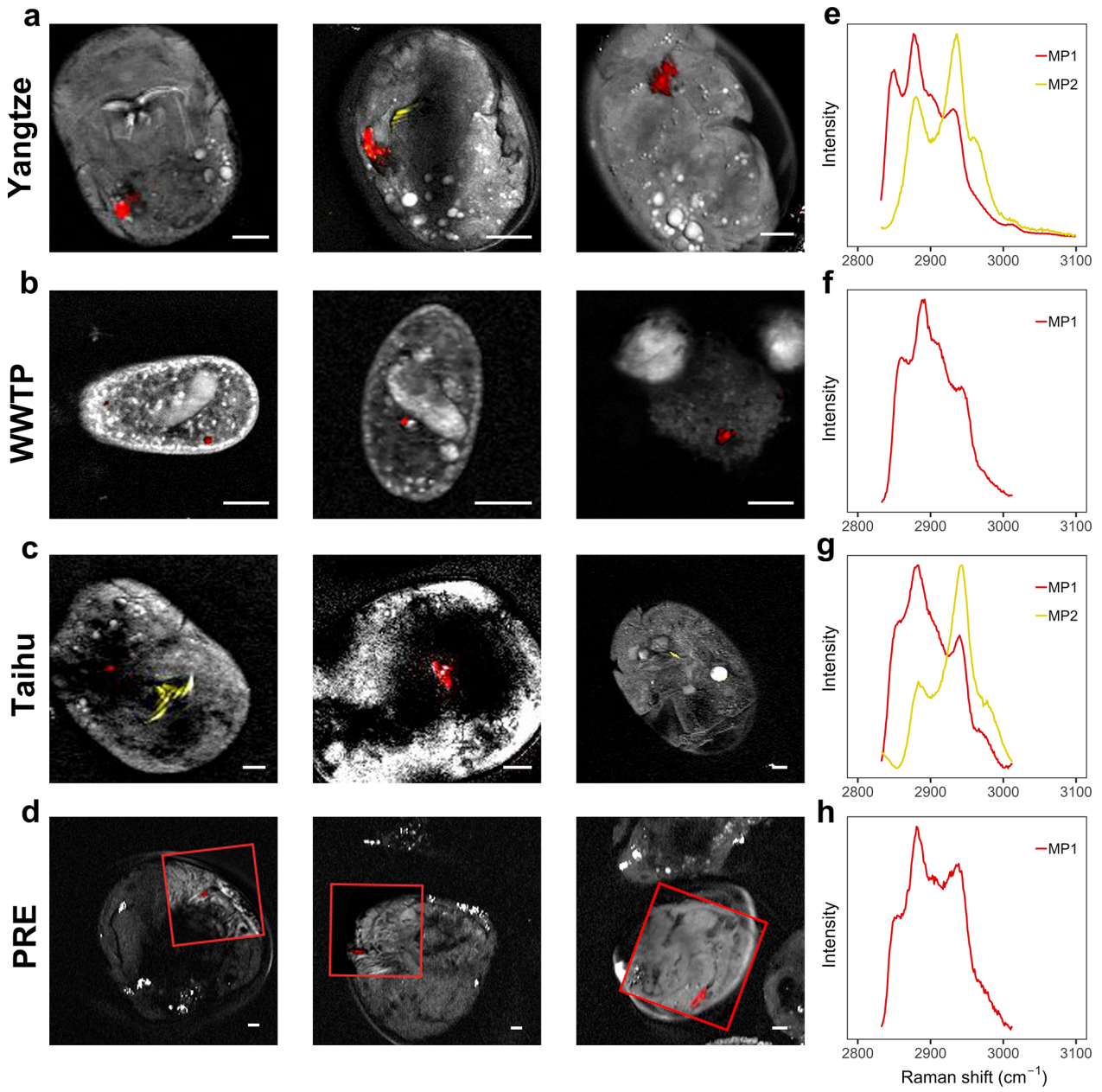

Figure 6. SRS imaging of protozoa collected from natural waters. (a–d) SRS images of the protozoan cells from water samples of Yangtze River (a), Xianlin Wastewater Treatment Plant (WWTP) (b), Lake Taihu (c), and the Pearl River Estuary (PRE) (d). (e–h) SRS spectra of the first (MP1) and second (MP2) types of MP as seen in the SRS images (a–d). While the SRS spectrum of MP1 can be clearly identified as PE, the spectrum for MP2 is less clear-cut. Spectrum-matching results from PublicSpectra (https://publicspectra.com/) revealed that MP2 could be nylon 46, thermoplastic polyester elastomer, acrylic rubber, or polyether block amide. In contrast to (a–c), the whole SRS image of (d) cannot be decomposed by the MCR algorithm. Therefore, only the red boxed area in (d) was processed by MCR. Scale bars, 10 μm.

(Figure 5d). Cellular concentration of PS-MPs determined by flow cytometry also correlated linearly with the exposure time (Figure S4a) and the cellular concentration of PS-MPs obtained by SRS (Figure S4b). Together, these results demonstrate that besides imaging, SRS can also quantify bioaccumulation of MPs.

SRS Imaging of MPs in Protozoa from Natural Waters. Encouraged by the laboratory observations, we used SRS to examine whether bioaccumulation of small MPs (<10 μm) occurs in protozoa from field samples. We collected and examined water samples from four representative aquatic systems: the Yangtze River, a wastewater treatment plant, Lake Taihu, and the Pearl River Estuary (see Materials and Methods and Figure S1 for detailed information on sampling sites). In contrast to conventional Raman spectroscopy, SRS is a nonresonant technique and its signal is not interfered by fluorescence.[47] Nevertheless, the pump–probe signal from the sample with strong fluorescence may still cause significant interference.[48] In the present study, some phytoplankton were collected, which could not be detected by SRS due to their strong pump–probe signals, but most of the protozoa can be clearly imaged by SRS.

All four sites showed similar MP bioaccumulation. Among the ~150 protozoan cells examined for each site (Figure S5), MPs were consistently detected inside 3–8 cells (~2–5%) (Figure 6). SRS imaging (Figure 6a–d) and spectra (Figure 6e–h) identified two types of MPs: MP1 and MP2. Out of 12

https://doi.org/10.1021/acs.est.3c07486
Environ. Sci. Technol. 2024, 58, 2922–2930

protozoan cells shown in Figure 6a−d, MP1 were found in 11 and MP2 were in three cells. While the SRS spectrum of MP1 can be clearly identified as PE (Figure 2a and Figure S2), the spectrum for MP2 is less clear-cut. Spectrum-matching results from PublicSpectra (https://publicspectra.com/) revealed that MP2 could be nylon 46, thermoplastic polyester elastomer, acrylic rubber, or polyether block amide. Besides protozoan cells, water samples collected from the Yangtze River also contained unknown cell aggregates or blastula whose surfaces were covered with PE-MPs. Copepod neonates from the estuary water also contained PE-MPs (Figure S6). Together, our results show bioaccumulation of MPs in microorganisms is ubiquitous across different aquatic systems including freshwater, wastewater, and seawater.

Although our SRS system offers the spectral information and resolution required to detect MP < 10 μm in microorganisms, its current throughput is very low as the SRS spectra between 2800 and 3100 cm^{-1} (instead of a single wavenumber) from each pixel of the target organism are collected. Further, because each cell needs to be examined manually under the microscope, inspecting 100 protozoan cells for MPs takes around 1−2 days. At this rate, it is less likely that other MPs will be detected, especially if their concentrations are much lower than those of PE. Increasing the throughput of the method in the future could increase the likelihood of detecting other types of MPs in the protozoa and improve the accuracy of the protozoan population that contains MPs (e.g., the proportion of MP-containing cells or the ratio of the area of pixels identified as MPs to the area of pixels identified as cells). Accurate data on MP bioaccumulation in protozoa could serve as an indicator of the concentration of small MPs in the natural environment. Moreover, if the throughput is highly improved, we can perform a systematic study about the spatiotemporal pattern for the accumulation of MPs in protozoan and also other organisms in natural waters.

Additionally, potential changes in the Raman spectra of weathered MPs in the natural environment should also be paid attention to. In fact, MP weathering is a challenge to all the detection methods such as Raman scattering, FT-IR, and also the mass spectrometry based technique. Theoretically, it would be better to collect different MP samples from the environment and build a database for weathered MPs, which could improve the accuracy of MP identification. In the present study we performed a hyperspectral mapping for the whole field of view and the SRS spectra between 2800 and 3100 cm^{-1} of each pixel of the image were obtained. Under this condition, we can identify the MPs not only based on their signal peak but also based on the shape of their spectra. Therefore, as long as the chemical composition of the weathered MPs does not change that much (e.g., not transformed completely to other substances), we can still identify them based on the shape of their SRS spectra. This is another advantage of obtaining the SRS spectra of each pixel for the field of view of a sample instead of imaging at a single wavenumber.

In summary, we realized label-free imaging of multiple types of MPs in protozoan cells grown in the lab and obtained from the field. Our method, which identifies MPs by their SRS spectra, show protozoa and other organisms in various natural waters accumulate MPs < 10 μm. Consistent with world plastic production volumes,[14] PE was the most prevalent plastic found in the microorganisms. The low proportion of protozoan cells containing MPs < 10 μm in our study suggests that the concentration of small and ultrasmall MPs in natural waters is low as reported previously.[49] However, this could change over time as more plastics are produced, released, and fragmented in natural waters,[42,50] Higher concentrations of small (<10 μm) MPs in the environment could lead to greater accumulation in microorganisms like protozoa, which, in turn, could impact biogeochemical cycling. Further, because microorganisms are at the base of our food chain, accumulated MPs can enter the food chain and impact organisms at the higher trophic levels including humans. Given small MPs migrate more easily and exert significantly greater biological effects than large MPs, their potential environmental and health risks merit a closer look.

■ ASSOCIATED CONTENT

Supporting Information

The Supporting Information is available free of charge at https://pubs.acs.org/doi/10.1021/acs.est.3c07486.

Map of the sampling sites; physicochemical properties of different polymer types of MPs; scanning electron microscopy images of differently sized PS; uptake kinetics of PS during a 90 min period; bright-field images of the protozoan cells from natural waters; SRS imaging of cell aggregates collected from Yangtze River and the copepod neonate from the Pearl River Estuary (PDF)

Hyperspectral stack of 250 images at wavenumbers ranging from 2800 to 3100 cm (AVI)

■ AUTHOR INFORMATION

Corresponding Authors

Ping Wang − *Wuhan National Laboratory for Optoelectronics, Huazhong University of Science and Technology, Wuhan, Hubei Province 430074, China PRC;* orcid.org/0000-0002-5168-6829; Email: p_wang@hust.edu.cn

Ai-Jun Miao − *State Key Laboratory of Pollution Control and Resource Reuse, School of the Environment, Nanjing University, Nanjing, Jiangsu Province 210023, China PRC;* orcid.org/0000-0001-7681-2038; Email: miaoaj@nju.edu.cn

Authors

Mei Wang − *State Key Laboratory of Pollution Control and Resource Reuse, School of the Environment, Nanjing University, Nanjing, Jiangsu Province 210023, China PRC*

Zhiliang Huang − *Wuhan National Laboratory for Optoelectronics, Huazhong University of Science and Technology, Wuhan, Hubei Province 430074, China PRC*

Chao Wu − *State Key Laboratory of Pollution Control and Resource Reuse, School of the Environment, Nanjing University, Nanjing, Jiangsu Province 210023, China PRC*

Shuai Yan − *Wuhan National Laboratory for Optoelectronics, Huazhong University of Science and Technology, Wuhan, Hubei Province 430074, China PRC;* orcid.org/0000-0002-9083-7749

Hai-Tao Fang − *State Key Laboratory of Pollution Control and Resource Reuse, School of the Environment, Nanjing University, Nanjing, Jiangsu Province 210023, China PRC*

Wei Pan − *State Key Laboratory of Pollution Control and Resource Reuse, School of the Environment, Nanjing University, Nanjing, Jiangsu Province 210023, China PRC*

Qiao-Guo Tan − *Key Laboratory of the Coastal and Wetland Ecosystems of Ministry of Education, College of the Environment and Ecology, Xiamen University, Xiamen, Fujian 361102, China PRC;* orcid.org/0000-0001-9692-6622

https://doi.org/10.1021/acs.est.3c07486
Environ. Sci. Technol. 2024, 58, 2922−2930

Ke Pan − *Institute for Advanced Study, Shenzhen University, Shenzhen 518060, China PRC;* orcid.org/0000-0002-2931-1692

Rong Ji − *State Key Laboratory of Pollution Control and Resource Reuse, School of the Environment, Nanjing University, Nanjing, Jiangsu Province 210023, China PRC;* orcid.org/0000-0002-1724-5253

Liuyan Yang − *State Key Laboratory of Pollution Control and Resource Reuse, School of the Environment, Nanjing University, Nanjing, Jiangsu Province 210023, China PRC;* orcid.org/0000-0002-4211-006X

Bingcai Pan − *State Key Laboratory of Pollution Control and Resource Reuse, School of the Environment, Nanjing University, Nanjing, Jiangsu Province 210023, China PRC;* orcid.org/0000-0003-3626-1539

Complete contact information is available at: https://pubs.acs.org/10.1021/acs.est.3c07486

Author Contributions

[#]M.W. and Z.H. contributed equally to this paper.

Notes

The authors declare no competing financial interest.

■ ACKNOWLEDGMENTS

We thank three anonymous reviewers for their constructive suggestions on this paper. This work was supported by the National Key R&D Program of China (grant no. 2022YFA1205603), the National Natural Science Foundation of China (21822605, 22176093, and 21677068), and the Fundamental Research Funds for the Central Universities (021114380210).

■ REFERENCES

(1) Rochman, C. M.; Hoellein, T. The global odyssey of plastic pollution. *Science* **2020**, *368* (6496), 1184−1185.

(2) MacLeod, M.; Arp, H. P. H.; Tekman, M. B.; Jahnke, A. The global threat from plastic pollution. *Science* **2021**, *373* (6550), 61−65.

(3) Wright, S. L.; Kelly, F. J. Plastic and human health: a micro issue? *Environ. Sci. Technol.* **2017**, *51* (12), 6634−6647.

(4) Bar-On, Y. M.; Phillips, R.; Milo, R. The biomass distribution on Earth. *Proc. Natl. Acad. Sci. U. S. A.* **2018**, *115* (25), 6506−6511.

(5) Xu, S.; Wu, C.; Guo, W. B.; Yang, L.; Ji, R.; Pan, K.; Miao, A. J. Polystyrene nanoplastics inhibit the transformation of tetrabromobisphenol a by the bacterium *Rhodococcus jostii*. *ACS Nano* **2022**, *16* (1), 405−414.

(6) Wu, C.; Guo, W. B.; Liu, Y. Y.; Yang, L.; Miao, A. J. Perturbation of calcium homeostasis and multixenobiotic resistance by nanoplastics in the ciliate *Tetrahymena thermophila*. *J. Hazard. Mater.* **2021**, *403*, No. 123923.

(7) Ding, J.; Li, J.; Sun, C.; Jiang, F.; Ju, P.; Qu, L.; Zheng, Y.; He, C. Detection of microplastics in local marine organisms using a multi-technology system. *Anal. Methods.* **2019**, *11* (1), 78−87.

(8) Su, L.; Deng, H.; Li, B.; Chen, Q.; Pettigrove, V.; Wu, C.; Shi, H. The occurrence of microplastic in specific organs in commercially caught fishes from coast and estuary area of east China. *J. Hazard. Mater.* **2019**, *365*, 716−724.

(9) Kazour, M.; Jemaa, S.; Issa, C.; Khalaf, G.; Amara, R. Microplastics pollution along the Lebanese coast (Eastern Mediterranean Basin): occurrence in surface water, sediments and biota samples. *Sci. Total Environ.* **2019**, *696*, No. 133933.

(10) Yin, J.; Li, J. Y.; Craig, N. J.; Su, L. Microplastic pollution in wild populations of decapod crustaceans: a review. *Chemosphere* **2022**, *291*, No. 132985.

(11) Lim, X. Microplastics are everywhere—but are they harmful. *Nature* **2021**, *593* (7857), 22−25.

(12) Li, J.; Liu, H.; Paul Chen, J. Microplastics in freshwater systems: a review on occurrence, environmental effects, and methods for microplastics detection. *Water. Res.* **2018**, *137*, 362−374.

(13) Eerkes-Medrano, D.; Thompson, R. C.; Aldridge, D. C. Microplastics in freshwater systems: a review of the emerging threats, identification of knowledge gaps and prioritisation of research needs. *Water. Res.* **2015**, *75*, 63−82.

(14) Geyer, R.; Jambeck, J. R.; Law, K. L. Production, use, and fate of all plastics ever made. *Sci. Adv.* **2017**, *3* (7), No. e1700782.

(15) Auta, H. S.; Emenike, C. U.; Fauziah, S. H. Distribution and importance of microplastics in the marine environment: a review of the sources, fate, effects, and potential solutions. *Environ. Int.* **2017**, *102*, 165−176.

(16) Yan, N.; Tang, B. Z.; Wang, W. X. Cell cycle control of nanoplastics internalization in phytoplankton. *ACS Nano* **2021**, *15* (7), 12237−12248.

(17) Sun, X. D.; Yuan, X. Z.; Jia, Y.; Feng, L. J.; Zhu, F. P.; Dong, S. S.; Liu, J.; Kong, X.; Tian, H.; Duan, J. L.; Ding, Z.; Wang, S. G.; Xing, B. Differentially charged nanoplastics demonstrate distinct accumulation in *Arabidopsis thaliana*. *Nat. Nanotechnol.* **2020**, *15* (9), 755−760.

(18) Mitrano, D. M.; Beltzung, A.; Frehland, S.; Schmiedgruber, M.; Cingolani, A.; Schmidt, F. Synthesis of metal-doped nanoplastics and their utility to investigate fate and behaviour in complex environmental systems. *Nat. Nanotechnol.* **2019**, *14* (4), 362−368.

(19) Luo, Y.; Li, L.; Feng, Y.; Li, R.; Yang, J.; Peijnenburg, W. J. G. M.; Tu, C. Quantitative tracing of uptake and transport of submicrometre plastics in crop plants using lanthanide chelates as a dual-functional tracer. *Nat. Nanotechnol.* **2022**, *17* (4), 424−431.

(20) Jiang, X.; Tian, L.; Ma, Y.; Ji, R. Quantifying the bioaccumulation of nanoplastics and PAHs in the clamworm *Perinereis aibuhitensis*. *Sci. Total Environ.* **2019**, *655*, 591−597.

(21) Al-Sid-Cheikh, M.; Rowland, S. J.; Stevenson, K.; Rouleau, C.; Henry, T. B.; Thompson, R. C. Uptake, whole-body distribution, and depuration of nanoplastics by the *Scallop pecten* maximus at environmentally realistic concentrations. *Environ. Sci. Technol.* **2018**, *52* (24), 14480−14486.

(22) Schur, C.; Rist, S.; Baun, A.; Mayer, P.; Hartmann, N. B.; Wagner, M. When fluorescence is not a particle: the tissue translocation of microplastics in *Daphnia magna* seems an artifact. *Environ. Toxicol. Chem.* **2019**, *38* (7), 1495−1503.

(23) *Plastics − the Facts 2020. An analysis of European latest plastics production, demand and waste data*. PlasticsEurope, 2020; https://plasticseurope.org/knowledge-hub/plastics-the-facts-2020/.

(24) Lu, F. K.; Basu, S.; Igras, V.; Hoang, M. P.; Ji, M.; Fu, D.; Holtom, G. R.; Neel, V. A.; Freudiger, C. W.; Fisher, D. E.; Xie, X. S. Label-free DNA imaging in vivo with stimulated Raman scattering microscopy. *Proc. Natl. Acad. Sci. U S A* **2015**, *112* (37), 11624−11629.

(25) Hu, F.; Shi, L.; Min, W. Biological imaging of chemical bonds by stimulated Raman scattering microscopy. *Nat. Methods.* **2019**, *16* (9), 830−842.

(26) Hu, F.; Brucks, S. D.; Lambert, T. H.; Campos, L. M.; Min, W. Stimulated Raman scattering of polymer nanoparticles for multiplexed live-cell imaging. *Chem. Commun.* **2017**, *53* (46), 6187−6190.

(27) Huang, B.; Yan, S.; Xiao, L.; Ji, R.; Yang, L.; Miao, A. J.; Wang, P. Label-free imaging of nanoparticle uptake competition in single cells by hyperspectral stimulated Raman scattering. *Small* **2018**, *14* (10), No. 1703246.

(28) Zada, L.; Leslie, H. A.; Vethaak, A. D.; Tinnevelt, G. H.; Jansen, J. J.; de Boer, J. F.; Ariese, F. Fast microplastics identification with stimulated Raman scattering microscopy. *J. Raman Spectrosc.* **2018**, *49* (7), 1136−1144.

(29) Corliss, J. O. Have the protozoa been overlooked? *Bioscience* **2001**, *51* (6), 424−425.

(30) Finlay, B. J.; Esteban, G. F. Freshwater protozoa: biodiversity and ecological function. *Biodivers. Conserv.* **1998**, *7* (9), 1163−1186.

(31) Huang, Z.; Yan, S.; Li, Y.; Ju, W.; Wang, P. Direct counting and imaging chain lengths of lipids by stimulated Raman scattering microscopy. *Anal. Chem.* **2023**, *95* (13), 5815−5819.

(32) Laptenok, S. P.; Martin, C.; Genchi, L.; Duarte, C. M.; Liberale, C. Stimulated Raman microspectroscopy as a new method to classify microfibers from environmental samples. *Environ. Pollut.* **2020**, *267*, No. 115640.
(33) Wang, F.; Liu, G. Q.; Meng, H. L.; Guo, G.; Luo, S. J.; Guo, R. B. Improved methane hydrate formation and dissociation with nanosphere-based fixed surfactants as promoters. *ACS Sustain. Chem. Eng.* **2016**, *4* (4), 2107−2113.
(34) Gorovsky, M. A.; Yao, M. C.; Keevert, J. B.; Pleger, G. L. Isolation of micro-and macronuclei of *Tetrahymena pyriformis*. In *Methods Cell Biol.*; Elsevier: 1975; Vol. *9*, pp 311−327.
(35) Zhang, Y. X.; Wang, M.; Yang, L.; Pan, K.; Miao, A. J. Bioaccumulation of differently-sized polystyrene nanoplastics by human lung and intestine cells. *J. Hazard. Mater.* **2022**, *439*, No. 129585.
(36) Zhang, Q.; Liu, T.; Liu, L.; Fan, Y.; Rao, W.; Zheng, J.; Qian, X. Distribution and sedimentation of microplastics in Taihu Lake. *Sci. Total Environ.* **2021**, *795*, No. 148745.
(37) Wei, X.; Cai, S.; Zhan, W. Impact of anthropogenic activities on morphological and deposition flux changes in the Pearl River Estuary China. *Sci. Rep.* **2021**, *11* (1), 16643.
(38) *Standard operating procedure for zooplankton sample collection and preservation and secchi depth measurement field procedures*. United States Environmental Protection Agency, 2021; https://www.epa.gov/system/files/documents/2021-08/lg402a.v15-zooplankton-sampling_rfa.pdf.
(39) Wang, P.; Liu, B.; Zhang, D.; Belew, M. Y.; Tissenbaum, H. A.; Cheng, J. X. Imaging lipid metabolism in live *Caenorhabditis elegans* using fingerprint vibrations. *Angew. Chem.* **2014**, *126* (44), 11981−11986.
(40) Wang, C.; Zhao, J.; Xing, B. Environmental source, fate, and toxicity of microplastics. *J. Hazard. Mater.* **2021**, *407*, No. 124357.
(41) Xu, S.; Ma, J.; Ji, R.; Pan, K.; Miao, A. J. Microplastics in aquatic environments: occurrence, accumulation, and biological effects. *Sci. Total Environ.* **2020**, *703*, No. 134699.
(42) Koelmans, A. A.; Redondo-Hasselerharm, P. E.; Nor, N. H. M.; de Ruijter, V. N.; Mintenig, S. M.; Kooi, M. Risk assessment of microplastic particles. *Nat. Rev. Mater.* **2022**, *7* (2), 138−152.
(43) Isobe, A.; Iwasaki, S.; Uchida, K.; Tokai, T. Abundance of non-conservative microplastics in the upper ocean from 1957 to 2066. *Nat. Commun.* **2019**, *10* (1), 417.
(44) Ni, H.; Lin, P.; Zhu, Y.; Zhang, M.; Tan, Y.; Zhan, Y.; Wang, Z.; Cheng, J. X. Multiwindow SRS imaging using a rapid widely tunable fiber laser. *Anal. Chem.* **2021**, *93* (47), 15703−15711.
(45) Lv, X.; Gong, L.; Lin, S.; Jin, P.; Huang, Z. Super-resolution stimulated Raman scattering microscopy with the phase-shifted spatial frequency modulation. *Opt. Lett.* **2022**, *47* (17), 4552−4555.
(46) Nilsson, J. R. On Food Vacuoles in *Tetrahymena pyriformis* GL. *J. Protozool.* **1977**, *24* (4), 502−507.
(47) Freudiger, C. W.; Min, W.; Saar, B. G.; Lu, S.; Holtom, G. R.; He, C.; Tsai, J. C.; Kang, J. X.; Xie, X. S. Label-free biomedical imaging with high sensitivity by stimulated Raman scattering microscopy. *Science* **2008**, *322* (5909), 1857−1861.
(48) Malý, P.; Brixner, T. Fluorescence-detected pump−probe spectroscopy. *Angew. Chem., Int. Ed.* **2021**, *60* (34), 18867−18875.
(49) Xu, Y.; Ou, Q.; Jiao, M.; Liu, G.; van der Hoek, J. P. Identification and quantification of nanoplastics in surface water and groundwater by pyrolysis gas chromatography−mass spectrometry. *Environ. Sci. Technol.* **2022**, *56* (8), 4988−4997.
(50) Gigault, J.; El Hadri, H.; Nguyen, B.; Grassl, B.; Rowenczyk, L.; Tufenkji, N.; Feng, S.; Wiesner, M. Nanoplastics are neither microplastics nor engineered nanoparticles. *Nat. Nanotechnol.* **2021**, *16* (5), 501−507.

https://doi.org/10.1021/acs.est.3c07486
Environ. Sci. Technol. 2024, 58, 2922−2930